PHOTON INDUCED SECONDARY ELECTRON EMISSION

R. B. Spencer, TRW Systems Group; C. B. Smith, Norman Engineering Co.; and E. J. McGrath, Science Applications Inc.

This paper presents the results of numerical models for predicting photon induced secondary electron emission. These results are compared with recent experimental measurements made at UCLA using a Co-60 gamma ray source.

INTRODUCTION

An important consideration in the design of efficient spacecraft and missile radiation shielding is photon induced secondary electron emission. The secondary electrons may result in charge separation, thereby producing undesirable current flows and electromagnetic fields internal to the system. Basic to the prediction of such effects is a requirement to perform analyses for photon transport, electron production, and subsequent electron transport in arbitrary materials and geometries.

Electron emission from solids can be caused by high temperature, strong electric fields, and bombardment with photons and particles. Electrons emitted by primary electron bombardment are referred to as secondary electrons, and were discovered in 1902 by Austin and Starke[1] during a study of the reflection of electrons from metal. Austin and Starke observed that under certain circumstances more electrons were emitted than were incident on the material, indicating that the bombarding primary electrons ejected other electrons from the solid. Today the term "secondary electron emission" is used in a broader sense to indicate the phenomena of electron emission from solids subjected to bombardment from any type of particle or radiation. For the purpose of our study, the terms "secondary electron", and "secondary electron emission" are used with this broader meaning.

One phase of our study was a numerical investigation of the emission of secondary electrons from metals when the secondary electrons are produced by high-energy photons. A complete description of the secondary electron emission from the surface of a solid material is obtained when the number of electrons at a point in space as a function of energy is known. The function to be predicted is called the secondary electron current density and is denoted by $j_s(E,\Omega)$. The magnitude of the current density depends only on the states of interacting systems, i.e., on the properties of the primary beam and on the physical and chemical properties of the emitter, including chemical composition, crystal structure, surface conditions, and temperature. If $j_s(E,\Omega)$ is integrated over all energies and over all angles of the hemisphere surrounding an emitting planar surface, the total yield of secondary electrons is obtained. Much of the experimental work and theoretical work that has been performed in the past has been concerned with low-energy electrons (100 eV) as a source radiation. Recently, research has been directed at predicting secondary electron emission from solid materials using gamma ray sources emitting photons in the MeV energy range.

The purpose of our research is to improve the ability to predict the angular energy distributions of secondary electrons emitted from various types and thicknesses of materials exposed to photon radiation, and to develop and verify simplified calculational models for describing the phenomenon of secondary electron emission. These models provide a means of obtaining estimates of secondary electron emission produced by incident photons. The models were programmed on a digital computer to provide results for comparing with more sophisticated Monte Carlo programs and experimental results.

The computational models include one first proposed by Sawyer and Van Lint[2] and later refined by Spencer.[3] The Monte Carlo calculations were performed using the two-dimensional time dependent combined photon and electron code, TEMPER.[4]

We have performed experiments to measure the energy and angular distributions of secondary electrons emanating from several target materials.[3,5] Eight materials ($_{13}Al$, $_{22}Ti$, $_{29}Cu$, $_{42}Mo$, $_{48}Cd$, $_{73}Ta$, $_{82}Pb$ and $_{92}U$) ranging in thickness from 0.003" to 0.5" were used. The photon source used for the experiment was a 3 Ci Co^{60} source with photopeaks at 1.17 and 1.33 MeV. Pulse-height spectra (256 energy groups) of the emitted electrons were measured at 0, 10, 15, 20, 25, 30, 40, 50, and 60° to the beam forward direction for the gamma beam normal to the target.

A detection technique, proposed by Lonergan and Costello[6], which uses a transmission mounted Si semiconductor detector placed in front of a Pilot-B scintillator, was employed to discriminate against scattered incident photons. Since the semiconductor detector is only 131 microns thick, its efficiency for detecting scattered source photons is extremely low. By operating the two detectors in coincidence, the electron counts can be distinguished from

the photon counts in the scintillator. The thin semiconductor detector absorbs all electrons with energies less than about 160 keV, therefore only the high energy secondary electrons were measured for their energy and angular distributions. A complete description of the experimental measurements is given in References 3 and 5.

GENERAL SECONDARY ELECTRON EMISSION MODEL

The process of secondary electron emission consists of both the generation of the electrons and the transport, attenuation and eventual emission of the generated electrons. The concepts and details of electron transport in material have been considered using both analytical approximations and Monte Carlo numerical analysis. The majority of the electron transport theory that has been presented is based on the Boltzmann transport equation. The purpose of this paper is <u>not</u> to consider the Boltzmann equation for electrons, but rather to consider a simplified theory on which a numerical model of secondary electron emission could be based. The general secondary electron emission model described here is based on the model proposed by Sawyer and Van Lint.[2]

Figure 1 illustrates the geometry assumed in considering the general features of the secondary electron emission model. Consider a photon which is incident perpendicular to the surface of a slab target of thickness t. At a distance x before emerging from the target, the photon produces a secondary electron of kinetic energy T_i moving at an angle ϕ_i to the direction of the incident photon. The secondary electron loses energy and scatters in traveling through the remainder of the target, eventually emerging with kinetic energy T_f at an angle ϕ_f with the normal to the slab target. The purpose of the theory is to obtain an expression for the angular and energy distributions $N(T_f,\phi_f)$ of the emergent secondary electrons as a function of the target characteristics (atomic number and thickness) and the incident photon spectrum $\Phi_o(h\nu)$.

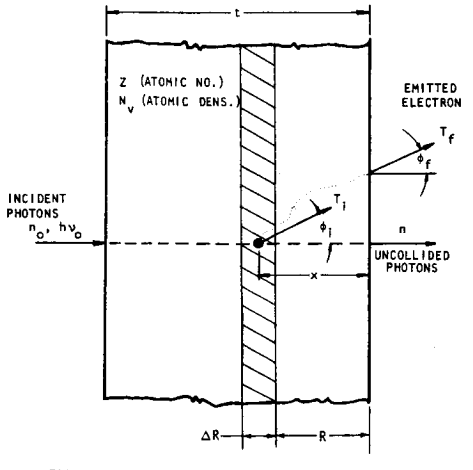

FIGURE 1. SLAB GEOMETRY FOR THIN ABSORBING SAMPLE

The total number of secondary electrons N_t generated within a thickness dx of the target, at a depth $t-x$, from photons of energy $h\nu$ is given by the product of the photon intensity at $t-x$, the electron production cross section, and the thickness dx.

$$N_t = [\text{photon intensity}]x[\text{electron production per photon per dx}]x[dx] \quad (1)$$

The number of secondary electrons of initial kinetic energy T_i within dT_i in solid angle $d\Omega'$ about initial angle ϕ_i is obtained by using the appropriate differential angular and energy electron production cross section.

$$N_{h\nu}(T_i,\phi_i)dT_i = [\Phi(h\nu,t-x)][ZN_v \frac{d\Omega'}{4\pi} \sigma(h\nu \rightarrow T_i,\phi_i)dT_i]dx \quad (2)$$

where:

$\Phi(h\nu,t-x)$ = photon intensity at $t-x$ with energy $h\nu$, photons

Z = atomic number of target material, electrons/atom

$N_v = \frac{\rho N_a}{A}$ atomic density of target material, atoms/cm^3

ρ = material density, g/cm^3

N_a = Avogadro's number = 0.6024×10^{24} atoms/g-atom

A = material atomic weight, g/g-atom

$\frac{1}{4\pi}\sigma(h\nu \rightarrow T_i,\phi_i)dT_i$ = the cross section per target electron for production of secondary electrons of energy T_i within dT_i, per unit solid angle near ϕ_i, cm^2/electron-steradian

$d\Omega' = \sin\phi_i d\phi_i d\psi$ = differential solid angle about ϕ_i, steradians

ψ = azimuthal angle of the generated secondary electrons

dx = material differential thickness, cm.

The energy spectrum of secondary electrons generated within a thin layer of thickness dx by a photon spectrum at the distance $t-x$ into the target, $\Phi(h\nu,x)$, is obtained by integrating $N_{h\nu}(T_i,\phi_i)$ over the range of energy of the incident photon spectrum.

$$N(T_i,\phi_i)dT_i = \int_0^{h\nu_{max}} \int_0^{2\pi} \Phi(h\nu,x)\, ZN_v \frac{1}{4\pi} \sigma(h\nu \rightarrow T_i,\phi_i) \cdot \sin\phi_i d\psi dh\nu d\phi_i dx\, dT_i \quad (3)$$

For a non-polarized incident photon spectrum, the secondary electron production is cylindrically symmetrical and integration over the azimuthal angle yields the following expression for the initial energy spectrum of the secondary electrons[2]

$$N(T_i,\phi_i)\,dT_i =$$

$$\frac{ZN_v}{2}\int_0^{h\nu_{max}} \Phi(h\nu,x)\sigma(h\nu\rightarrow T_i,\phi_i)\cdot \cdot \sin\phi_i dh\nu d\phi_i\,dx\,dT_i \qquad (4)$$

The transmission of a generated secondary electron to the back surface of the target can be described by a general probability function $p_e(T_i,\phi_i;\ x;\ T_f,\phi_f)$, which represents the probability per unit emerging energy T_f and solid angle Ω of escape with energy near T_f, and angle near ϕ_f for a secondary electron generated at a distance x below the surface with energy T_i and at angle ϕ_i. Including this probability function and indicating the integrations over the target thickness (t), energy of formation (T_i) and angle of formation (ϕ_i), the angular-energy distribution of emitted secondary electrons is[2]

$$N(T_f,\phi_f)dT_f d\Omega =$$

$$\frac{ZN_v}{2}\int_0^{h\nu_{max}}\int_0^{t}\int_0^{T_{i\ max}(h\nu)}\int_0^{\pi}\Phi(h\nu,x)\cdot \cdot \sigma(h\nu\rightarrow T_i,\phi_i)p_e(T_i,\phi_i;x;T_f,\phi_f)\cdot \cdot \sin\phi_i d\phi_i dT_i dx\,dh\nu\,dT_f d\Omega \qquad (5)$$

The photon intensity at each depth in the target and at each energy is related to the incident photon intensity by an exponential attenuation factor. An energy-dependent absorption coefficient $\mu_o(h\nu)$ is determined by the combined total cross sections for Compton scattering, photoelectric effect, and pair production interactions. The intensity of the energy-dependent uncollided photons at a depth t-x within the target is thus given by

$$\Phi(h\nu,t-x) = \Phi_o(h\nu)e^{-\mu_o(h\nu)(t-x)} \qquad (6)$$

where the contribution of multiple Compton scattering has been neglected.

Numerically, the energy-dependent photon attenuation and resulting photon intensity at a given target depth is calculated by means of a computer program called XRAY.[7] This code divides the incident photon spectrum into energy groups (up to 100) and obtains the energy dependent absorption cross section by means of table look-up. The total attenuation coefficients μ_o and energy absorption coefficients μ_a (for photon energies between 0.1 keV and 10 MeV) are contained on magnetic tape for about 50 of the most common elements. XRAY has the capability of handling multi-element, multi-region shields and can calculate the uncollided photon intensity, transmission factor, energy deposition, and absorbed dose in standard materials (e.g. rads Si) as a function of material depth for an arbitrary input photon spectrum.

If the assumption is made that the statistical fluctuation in the range of secondary electrons of the same initial energy is a Gaussian distribution about the mean range $\bar{R}$, the probability of escape $p_e(T_i,\phi_i;x;T_f,\phi_f)$ can be shown to be [2]

$$p_e = \frac{1}{2}\left[1-\mathrm{erf}\left(\frac{x/\cos\phi_i-\bar{R}(T_i)}{\alpha}\right)\right]\delta(\phi_i-\phi_f)\delta(T_f-\bar{T}) \qquad (7)$$

where α is the range-straggling parameter and is related to the standard deviation of the range-straggling Gaussian distribution by $\alpha = \sqrt{2}\,\delta$. The Dirac delta functions $\delta(\phi_i-\phi_f)$ and $\delta(T_f-\bar{T})$ connote, respectively, the assumptions that the final angle of emission ϕ_f is the same as the initial generation angle ϕ_i and the final energy T_f is equal to an average electron energy $\bar{T}$. $\bar{T}$ corresponds to the average range remaining to the electrons beyond the distance to the surface $x/\cos\phi_i$ for those electrons which penetrate. The first assumption presumes that multiple scattering of the secondary electrons does not, on the average, have a net effect on the direction of the generated electrons. The average energy of the emitted electrons $\bar{T}$ (all starting at the same energy T_i) is given by[2]

$$\bar{T} = \exp\left\{\frac{1.265-[1.6-0.3816\ln(\Delta R_e/0.273)]^{1/2}}{0.1908}\right\} \qquad (8)$$

for electrons with energies from 10 keV to 3 MeV. The ΔR_e in the expression for $\bar{T}$ is the increment of range from the emitting surface ($x/\cos\phi_i$) to the range R_e associated with the average energy of escape $\bar{T}$.

INVESTIGATION OF TWO SIMPLIFIED MODELS

Two simplified models were investigated in an attempt to obtain numerical results to compare with the results of experiments. The first model investigated is the model we call the "Average Angle and Energy Model" (AA model) or the "van Lint Model" since it is used essentially unmodified as proposed by Sawyer and van Lint.[2] The second model is a refinement of the AA model and gives a more realistic simulation of the secondary electron generation and emission phenomenon. We call this model the "Angle-Bin Model" (AB model). Both of these models are based on the previous equations, but differ in the details of the calculations.

Average Angle and Energy Model

The main feature of the AA model can best be described by referring to Figure 1. In this figure, the angle between the electron's initial direction and the normally incident photon is labeled ϕ_i. In the AA model, ϕ_i is taken to be the average angle, $\bar{\phi}_i$, of all the electrons produced by the photons (in a particular energy group) for the Compton scattering interaction. The $\bar{\phi}_i$ are obtained by first calculating the average energy of the recoil Compton electron

(i.e., the secondary electron). The relation for the average energy recoil Compton electron for the photons of energy group i is given by

$$\bar{T}_i = (\overline{h\nu_o})_i \frac{e^{\sigma_a}(\overline{h\nu_o})_i}{e^{\sigma}(\overline{h\nu_o})_i} \quad (9)$$

where:

$\bar{T}_i$ = the average initial energy of the recoil Compton electron for photons of energy $\overline{h\nu_o}$ (in group i).

$e^{\sigma_a}(\overline{h\nu_o})_i$ = the average Compton absorption cross section for photons of energy $\overline{h\nu_o}$ (in group i).

$e^{\sigma}(\overline{h\nu_o})_i$ = the average Compton collision cross section for photons of energy $\overline{h\nu_o}$ (in group i).

Once the average secondary electron energy $\bar{T}_i$ is evaluated, the average direction cosine of the secondary electron in terms of the average photon energy of group i can be obtained:

$$\cos \bar{\phi}_i \simeq \overline{\cos}\ \phi_i \simeq \sqrt{\frac{\bar{T}_i\,(1+\alpha_i)^2}{\bar{T}_i\alpha_i^2 + 2\alpha_i(\overline{h\nu_o})_i}} \quad (10)$$

where: $\cos \bar{\phi}_i$ = the cosine of the average initial angle of the Compton recoil electron

$\overline{\cos}\ \phi_i$ = the average cosine of the initial angle of the Compton recoil electron

$\alpha_i = (\overline{h\nu_o})_i / m_o c^2$

The actual distance the electron must travel to escape, R, (assuming that the average direction of the electron does not change during its transport) is given by

$$R = X_n / \overline{\cos}\ \phi_i \quad (11)$$

where: X_n is the distance from the centerline of the appropriate ΔR to the escaping surface (shortest distance).

Numerically, this process is repeated for all of the photon energy groups and for all X_n or ΔR's comprising the target, so that the number of secondary electrons at each angle and the energies of the escaping electrons can be accumulated for small ranges of angle and energy, called "bins." The resulting accumulated secondary electron energy and angular distributions are then printed to give the final results.

Angle-Bin Model

The AB model also uses the same basic equations given previously. However, instead of using the average electron angle ϕ_i to represent the initial direction of the generated electrons, all possible angles in the forward direction are represented by dividing the quadrant into equal angle bins. The cross sections are then calculated for each angle bin.

For the Compton scattering interaction, the cross section for scattering an electron into each angle bin is obtained by integrating the differential scattering cross section over the range of angles for the particular angle bin. The average energy of the electron scattered into an angle bin is calculated using the simple average angle of the bin as $\bar{\phi}$, i.e., $\bar{\phi} = (\phi_1 + \phi_2)/2$. Numerically, the AB model is implemented by using Gaussian quadrature sets for the required integrations.

The results of the numerical calculations from the subroutine that calculates the cross sections for Compton scattering were compared with the results as calculated by Nelms.[8] The curves presented in the report by Nelms were graphically integrated to verify the numerical integrations of the Compton cross sections.

The final results of the AB model are obtained by computing the Compton scattering contribution to the secondary electron emission. Once the secondary electrons have been generated for a particular angle bin, the subsequent transmission, attenuation and emission is numerically performed in the same manner as the secondary electrons in the average angle (AA) model, except that a separate calculation is required for each angle bin.

Numerical Results

Numerical calculations were performed using the AA and AB models for a typical target configuration and using the gamma ray energy spectrum measured for the experimental source (see Figure 2). The AA and AB models were incorporated into the existing XRAY[7] program as subroutines. The XRAY program calculated the attenuated photon spectrum within the target material and then the AA and AB model subroutines were used to calculate the generation of high energy secondary electrons (initial angular and energy distributions) and the subsequent transmission, attenuation, and emission of the secondary electrons.

FIGURE 2. INCIDENT PHOTON ENERGY SPECTRUM

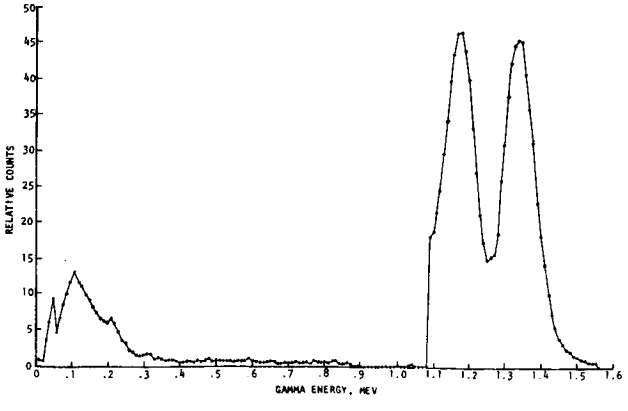

The results of the calculations for a 140 mil (0.355 cm or 3.18 g/cm^2) thick copper target (density = 8.96 g/cm^3) are shown in Figures 3 through 8. Figure 3 is the angular distribution of the emitted secondary electrons as calculated by the AA model. This figure shows the angular distribution for electrons of all energies. The range of angles represented is small (28° to 47°) because the average angle was selected for each photon energy group. For the AA model, it is not surprising that this comparatively small range of angles represented the angular distribution of the emitted secondary electrons.

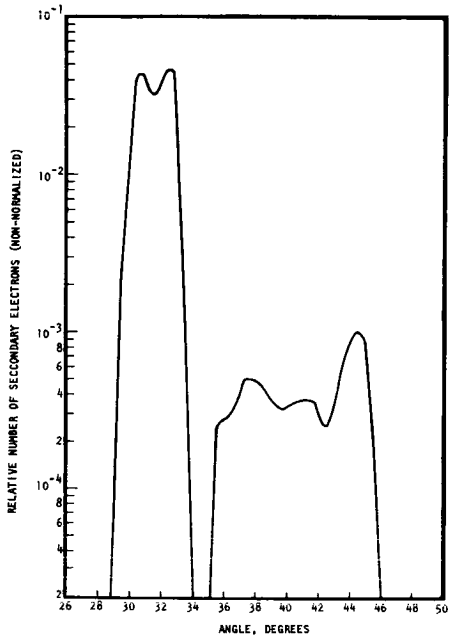

FIGURE 3. AA MODEL ANGULAR DISTRIBUTION

Figure 4 is the energy distribution of the emitted secondary electrons that was calculated by the AA model. This distribution represents the energy distribution for all secondary electrons emitted from the back surface (i.e., photon beam forward direction) of the copper target. It is expected that secondary electrons would have low energies since the attenuation of electrons produced relatively deep in the target is calculated by using range-energy relations. In addition, since the AA model considers only the Compton scattering event, and considers average angles (and the resulting average energy at that angle), energies greater than approximately 0.8 MeV are not represented in the energy distribution.

Figure 5 contains the angular energy distributions for the emitted secondary electrons as calculated by the AB model for constant angles of 10°, 20°, 30°, 40° and 50°. The striking feature of these curves is that the general shape of the incident photon energy spectrum is clearly evident for each particular emission angle. The shift to lower energy secondary electrons with increasing emission angle is also clearly seen. This shift is a result of the Compton scattering event since the closer the secondary electron is to 90° to the incident photon, the less energy is imparted to the electron. The angular distributions for both the Compton scattering and photoelectric effect cross sections were obtained for the AB model. However, the number of secondary electrons emitted as a result of the photoelectric effect was negligible compared to the number of Compton scattering electrons and thus only the Compton scattering electrons have been

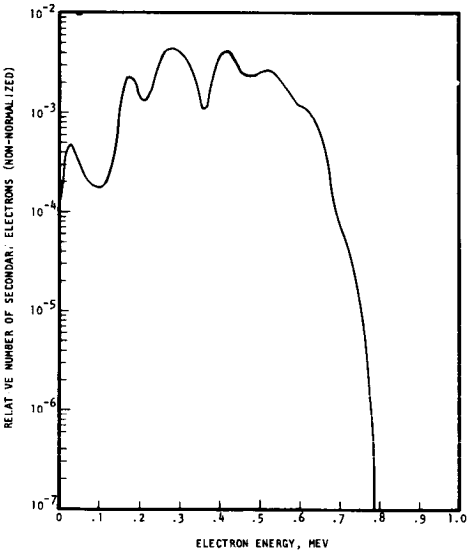

FIGURE 4. AA MODEL ENERGY DISTRIBUTION

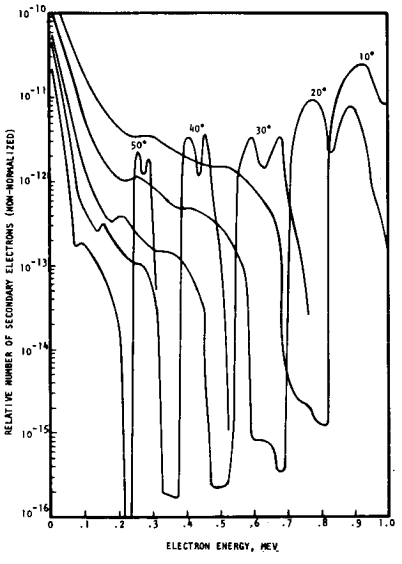

FIGURE 5. AB MODEL ANGULAR ENERGY DISTRIBUTION

plotted. This is not surprising since the photoelectric effect cross section is negligible compared to the Compton scattering cross section for the predominate range of photon energies represented by the incident gamma ray spectrum (most are around the 1.1 to 1.4 MeV range as shown in Figure 2.)

Figure 6 is a cross-plot of Figure 5 and reveals the erratic behavior of the detailed angular energy distributions for the emitted secondary electrons as calculated via the AB model. Figures 7 and 8 are the energy and angular distributions as calculated using the AB model for the secondary electrons emitted from the copper target. These distributions were obtained by integrating the angular energy distributions and the energy angular distributions of Figures 5 and 6, respectively. The similarity in shape of the AA model and AB model energy distributions (Figures 4 and 7) is clearly seen. The major difference is that the secondary electrons calculated by the AB model cover a wider range of energy. This is expected since the AA model considers only the "average" secondary electron energy for any given photon energy group, whereas the AB model accounts for the entire range of energies of the generated secondary electrons by employing angle and energy bins.

Based on the numerical results presented here, the AB model is concluded to be a more realistic method of calculating secondary electron emission. The AB model can readily indicate the detailed angular energy distributions and the energy angular distributions, as well as the angular and energy distributions of the emitted secondary electrons.

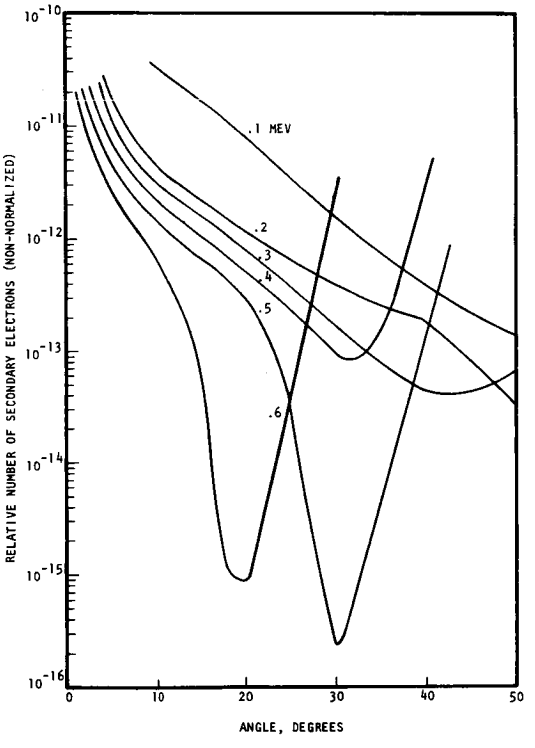

FIGURE 6. AB MODEL ENERGY ANGULAR DISTRIBUTIONS

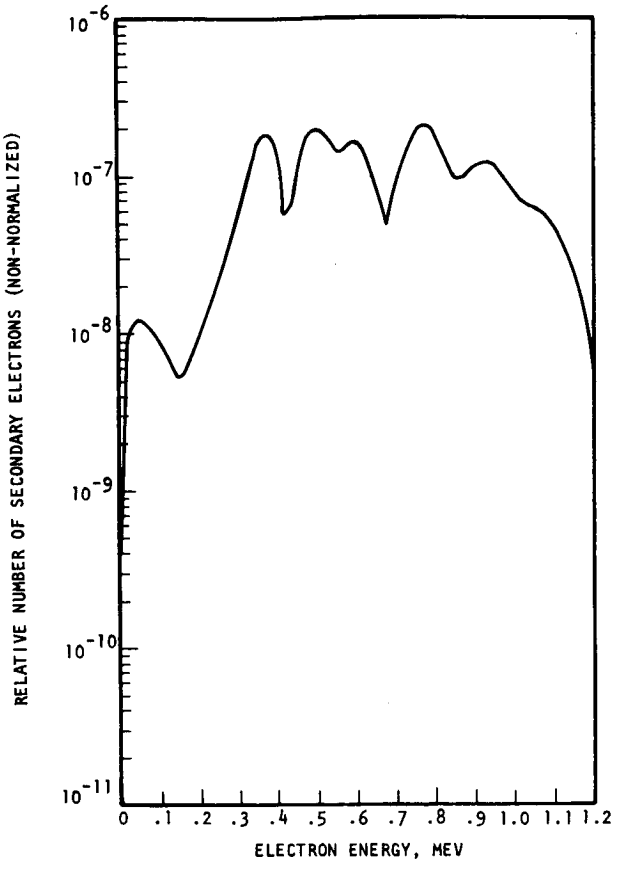

FIGURE 7. AB MODEL TOTAL ENERGY DISTRIBUTION

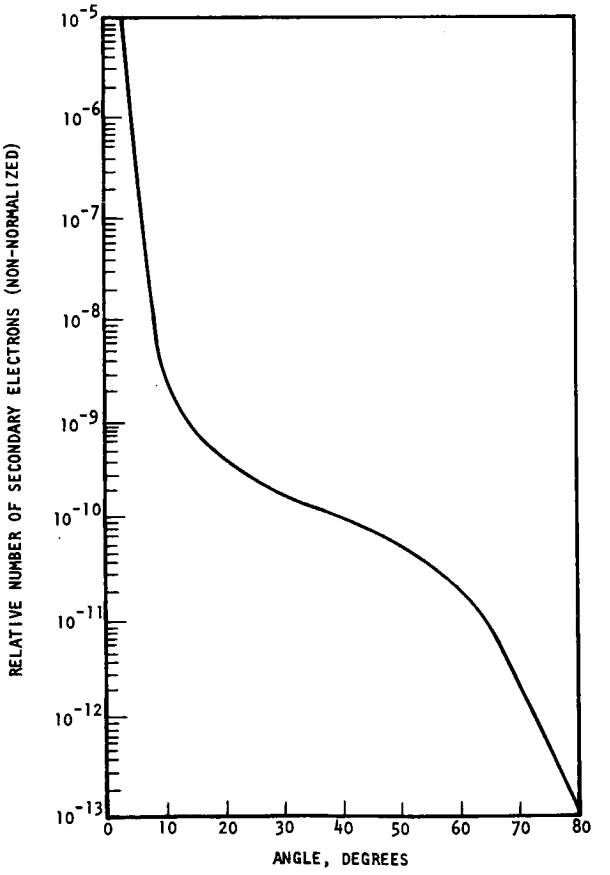

FIGURE 8. AB MODEL TOTAL ANGULAR DISTRIBUTION.

COMPARISON OF EXPERIMENTAL AND NUMERICAL RESULTS

The total angular and total energy secondary electron distributions are well suited for comparing numerical and experimental results. These distributions have many of the detailed anomalies integrated out for both the numerical and experimental results.

Figure 9 shows the AB model numerical results for the secondary electron total energy distribution of a 3.2 g/cm^2 thick copper target. Superimposed on this graph are the reduced experimental data for the same thickness copper target. The experimental data have been normalized to the numerical results at the 1.0 MeV energy point. There is generally fair agreement in the results from 0.4 MeV to 1.2 MeV. The experimental data do not possess the detailed variations that the numerical results indicate. The major reason for this relative smoothness of the experimental data compared to the numerical results is the poor resolution of the scintillation crystal detector. The calibration tests of the scintillation detector using a standard conversion electron emitter source (Cs^{137} with a 0.624 MeV conversion electron) showed that the resolution of the detector was approximately 20% (i.e., full width at half maximum), or about twice what is considered average resolution.

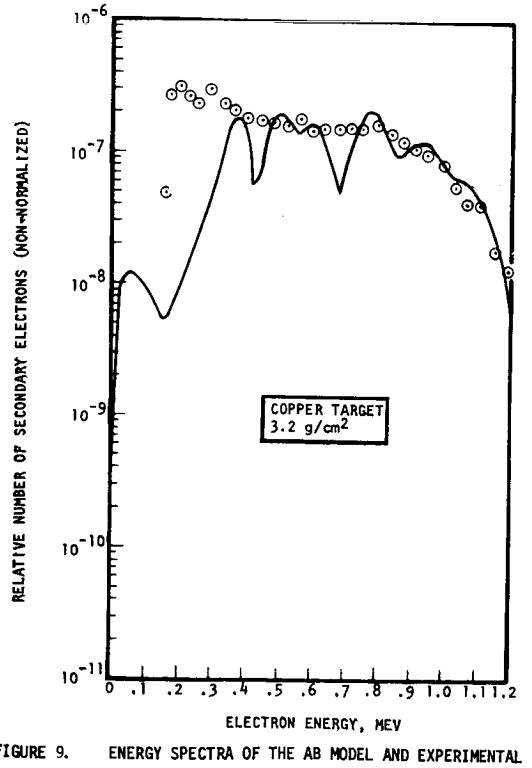

FIGURE 9. ENERGY SPECTRA OF THE AB MODEL AND EXPERIMENTAL RESULTS.

The secondary electron total angular distribution as calculated by the AB model was presented in Figure 8 for the 3.2 g/cm^2 thick copper target. This graph is shown in Figure 10 along with the reduced data for the same thickness target. The experimental data are normalized to the numerical results at the 20 degree point. The AB model results and the experimental data do not agree well for angles less than 10°. The primary reason for this is that the AB model does not account for the change in the initial angular distribution of the photon generated secondary electrons as they are scattered through the remainder of the target material. In reality, the generated electrons are highly scattered before they are emitted and, thus, the experimentally measured emitted electron angular distribution tends to be more uniform than the calculated distribution. Another reason for the difference at the low angles (<10°) is that the experimental data were subject to a high background.

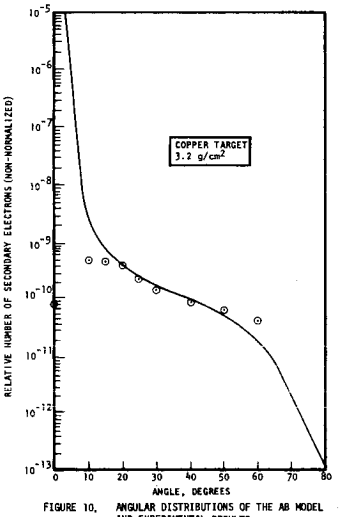

FIGURE 10. ANGULAR DISTRIBUTIONS OF THE AB MODEL AND EXPERIMENTAL RESULTS.

Comparisons with more detailed results than those obtained using the simplified AB model may indicate areas where improvements in the simplified model can be made. Several computer runs were made using the TEMPER[4] code. The TEMPER computer program was developed to solve radiation transport problems with a specified electron or photon source and to include any secondary radiations in the solution.[4] The program is well suited for the investigation of secondary electron emission since it calculates the actual energy deposition in thin samples where the secondary electrons escape from the sample. Among the more important features of the computer program are: The Monte Carlo method is used for the transport of photons and electrons; radiation sources are arbitrary functions of energy, time, space and angle; the material distributions are generalized three-dimensional volumes; and detailed angular and energy distributions are computed for volume, surface and point detectors.[4]

The TEMPER program was run for the 3.2 g/cm^2 thick copper target using two equal intensity monoenergetic photon sources at 1.17 MeV and 1.33 MeV. Figure 11 is the plot of the TEMPER numerical results for the total energy distribution of the emitted secondary electrons at the back surface of the target material. This energy distribution does not compare well with the AB model numerical results shown in Figure 9. One possible explanation for this discrepancy may be the fact that the TEMPER calculations did not have any low energy photons incident on the target and, thus, the energy distribution tended to peak at a higher energy (∿.7 MeV). The lower energy photons would tend to produce more photoelectrons with energies close to the incident photon energy.

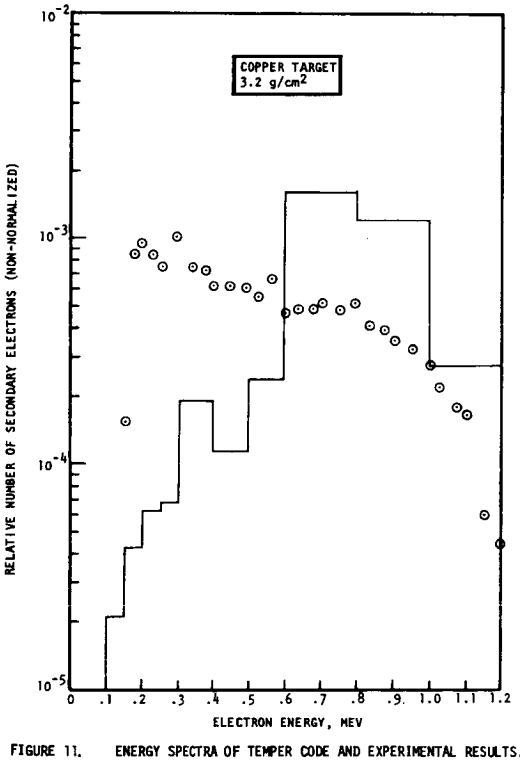

FIGURE 11. ENERGY SPECTRA OF TEMPER CODE AND EXPERIMENTAL RESULTS.

Fair agreement is found for the secondary electron total angular distributions as calculated by TEMPER and as obtained from the reduced experimental results. Figure 12 presents the TEMPER results and experimental results for the 3.2 g/cm^2 thick copper target with the experimental results normalized to the TEMPER results at 20 degrees. A slight decrease in the number of secondary electrons for angles less than about 15° is indicated from the TEMPER results. The reduced experimental results show that a relatively constant number of secondary electrons are emitted between 10° to 20° with a decrease below 10°.

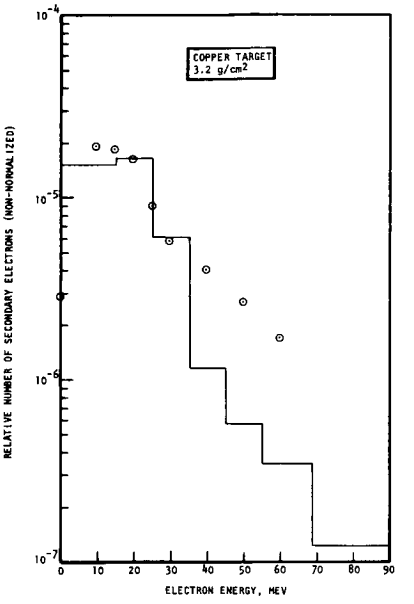

FIGURE 12. ANGULAR DISTRIBUTIONS FOR THE TEMPER CODE AND EXPERIMENTAL RESULTS.

In summary, the comparison of the reduced experimental results with the results obtained using the simplified AB model and a refined Monte Carlo code (TEMPER) indicated the following: 1) The AB model reasonably predicts the shape of the secondary electron total energy distribution for electrons with energies greater than 0.4 MeV, but this model is unsatisfactory in evaluating the shape of the angular distribution for angles less than 15°. 2) The TEMPER results indicate the general trend of the total angular distribution, but these numerical results do not compare well for the energy distribution of emitted secondary electrons.

CONCLUSIONS

An evaluation has been made of a few analytical models used for predicting the details of photon induced secondary electron emission. The results from both simplified and more sophisticated (Monte Carlo) methods have been compared with recent experimental measurements using a Co-60 gamma source and a unique detection technique for measuring the energy and angular distributions of secondary electrons. The results of the evaluation indicated that the two simplified models are useful only for idealized situations. These models did not adequately account for the detailed and complex transport of the generated secondary electrons within the target materials. The multiple and large angle catastrophic collisions that electrons can experience in traversing media must be accounted for to accurately predict the angular and energy distributions of the emitted secondary electrons. Therefore, more refined calculational procedures (e.g., discrete ordinate S_n, Monte Carlo or other analytical techniques) for dealing with the details of electron transport appear warranted.

REFERENCES

1. AUSTIN, L. and STARKE, H.,"Reflection and Secondary Emission of Kathode Rays," Ann. Physik, Vol. 9, 1902, pp. 271.
2. SAWYER, J.A., and VAN LINT, V.A.J., "Calculation of High-Energy Secondary Electron Emission," J. Appl. Phys., Vol. 35, No. 6, June 1964, pp. 1706-1711.
3. SPENCER, R.B., "Measurement of Photon-Induced High-Energy Secondary Electron Emission," Ph.D. Dissertation, University of California, School of Engineering and Applied Science, Los Angeles, 1970.
4. JORDAN, T.M., "TEMPER, A Computer Program for the Transport in Electro Magnetic Fields of Photon and Electron Radiation by Monte Carlo and Finite Difference Techniques," Report No. ART-33, A.R.T. Research Corp., Los Angeles, California, July 1969.
5. SPENCER, R.B. and SMITH, C.B., "An Experimental Investigation of Photon-Induced Secondary Electron Emission," Trans. Am. Nuc. Soc., Vol. 13, No. 1, June 1970.
6. LONERGAN, J.A. and COSTELLO, D.G., "Energy and Angular Distribution of Electrons Transmitted through Tin," Trans. Am. Nuc. Soc., Vol.12 No. 1, June 1969.
7. SPENCER, R.B., "XRAY Program User's Manual," Report No. AN031C, TRW Systems Group, Redondo Beach, California, December 1968.
8. NELMS, A.T., "Graphs of the Compton Energy-Angle Relationship and the Klein-Nishina Formula from 10 KeV to 500 MeV," National Bureau of Standards Circular 542, Washington D.C., August 28, 1953.